Virology 454-455 (2014) 311–327

Contents lists available at ScienceDirect

Virology

journal homepage: www.elsevier.com/locate/yviro

Varicella-zoster virus induces the formation of dynamic nuclear capsid aggregates

Marielle Lebrun [a], Nicolas Thelen [b], Marc Thiry [b], Laura Riva [a], Isabelle Ote [a,1], Claude Condé [a], Patricia Vandevenne [a,2], Emmanuel Di Valentin [c], Sébastien Bontems [a,3], Catherine Sadzot-Delvaux [a,*]

[a] University of Liege (ULg), GIGA-Infection Immunity and Inflammation, Laboratory of Virology and Immunology, Liege, Belgium
[b] University of Liege (ULg), GIGA-Neurosciences, Laboratory of Cellular and Tissular Biology, Liege, Belgium
[c] University of Liege (ULg), GIGA-Viral Vectors Platform, Liege, Belgium

ARTICLE INFO

Article history:
Received 30 September 2013
Returned to author for revisions
21 October 2013
Accepted 21 February 2014
Available online 28 March 2014

Keywords:
Herpesvirus
VZV
ORF23
VP26
UL36
UL37
Fluorescent virus
Assembly
Capsid
Correlative microscopy

ABSTRACT

The first step of herpesviruses virion assembly occurs in the nucleus. However, the exact site where nucleocapsids are assembled, where the genome and the inner tegument are acquired, remains controversial. We created a recombinant VZV expressing ORF23 (homologous to HSV-1 VP26) fused to the eGFP and dually fluorescent viruses with a tegument protein additionally fused to a red tag (ORF9, ORF21 and ORF22 corresponding to HSV-1 UL49, UL37 and UL36). We identified nuclear dense structures containing the major capsid protein, the scaffold protein and maturing protease, as well as ORF21 and ORF22. Correlative microscopy demonstrated that the structures correspond to capsid aggregates and time-lapse video imaging showed that they appear prior to the accumulation of cytoplasmic capsids, presumably undergoing the secondary egress, and are highly dynamic. Our observations suggest that these structures might represent a nuclear area important for capsid assembly and/or maturation before the budding at the inner nuclear membrane.

Introduction

Varicella-zoster virus (VZV) is a human pathogen belonging to the alphaherpesviruses subfamily, whose most characterized member is the human Herpes Simplex Virus-1 (HSV-1). VZV causes varicella as primary infection and zoster when the virus eventually reactivates (Arvin, 1996).

The first steps of herpesviruses virion assembly occur in the nucleus where the replicated DNA must be embedded into the preformed capsids. It is quite well established that the replication starts at specific spots that increase over time, in number and mainly in size, until they finally fuse to give rise to what has been called the "replication compartment" (RC) (de Bruyn Kops and Knipe, 1994; Kobiler et al., 2011; Quinlan et al., 1984).

HSV-1 capsid assembly is well documented (for review see Cardone et al., 2012; Homa and Brown, 1997). In the nucleus, the subunits are assembled into procapsids around a protein scaffold containing the products of two overlapping in-frame genes, UL26 (VZV ORF33) and UL26.5 (VZV ORF33.5) (Thomsen et al., 1995). The polypeptide encoded by UL26 (VP24+pre-VP21) shares its C-terminal part with the one coded by UL26.5 (pre-VP22a), but possesses an extra N-terminal part consisting of a protease motif and a linker peptide. Once the procapsid is formed, the protease motif (VP24) becomes activated and frees itself through an autocatalytic cleavage. The activated VP24 gives then rise to mature VP21 and VP22a via another proteolytic cleavage at the C-terminal end of both precursors (Newcomb et al., 2000). Procapsids are thought to be transient intermediates at the origin of the three types of capsid that are generally found in the nucleus of an infected cell. Capsids A, B and C share the outer shell composed of capsomers of VP5 (homologous to VZV ORF40) linked via a triplex containing two molecules of VP23 (VZV ORF41) and

* Corresponding author. Mailing address: Laboratory of Virology and Immunology, University of Liege, Avenue de l'Hopital 1, GIGA-R, B34 (+5), B-4000 Liege, Belgium. Tel.: +32 4 366 24 45; fax: +32 4 366 41 98.
E-mail address: csadzot@ulg.ac.be (C. Sadzot-Delvaux).
[1] Present address: Coris BioConcept, Science Park CREALYS, Rue Jean Sonet 4A, B-5032 Gembloux, Belgium.
[2] Present address: Institute for Medical Immunology, ULB, Rue Adrienne Bolland 8, B-6041 Gosselies, Belgium.
[3] Present address: AIDS Reference Laboratory, CHU, ULG, B23, Avenue de l'hopital 1, B-4000 Liege, Belgium.

http://dx.doi.org/10.1016/j.virol.2014.02.023
0042-6822

one of VP19C (VZV ORF20) and decorated by the small capsid protein VP26 (VZV ORF23) (Spencer et al., 1998). The inside of the capsid is either empty (type A) when the expulsion/degradation of the scaffold is not followed by DNA insertion, filled with DNA (type C) or filled with truncated VP22a (type B), which is a scaffold remnant resulting from cleavage by the viral protease during the encapsidation process (Newcomb et al., 1996; Salmon et al., 1998) (for review see Cardone et al., 2012).

The exact place where the replicated DNA is cleaved and encapsidated and where the capsid acquires its inner and outer tegument is still a matter of debate (de Bruyn Kops et al., 1998; Taus et al., 1998). Immunofluorescence using specific antibodies and, more recently, the fusion of viral genes with genes coding for fluorescent proteins coupled with confocal microscopy have significantly helped to decipher the complex virion formation process from the nuclear steps to the final egress at the cell surface (de Oliveira et al., 2008; Luxton et al., 2005; Smith et al., 2004; Sugimoto et al., 2008). Early in infection, capsid proteins are frequently found in the replication compartment, whereas later time points are characterized by the appearance of very dense structures localized at the periphery of the RC. These structures comprise both mature and immature capsid proteins as well as some tegument proteins and have been called "assemblons" (Ward et al., 1996). Their potential role in the infection process is controversial, as they could either be a functional compartment highly specialized in nucleocapsid formation or a depot of dead-end products resulting from a protein excess (Abaitua and O'Hare, 2008; Hutchinson et al., 2002; Lee et al., 2006; Markovitz and Roizman, 2000; Ward et al., 1996).

We know little about VZV nucleocapsid formation, but, based on HSV-1 homology, one should expect a similar process, even though some peculiar features, like the nuclear import of capsid subunits, have already been described (Chaudhuri et al., 2008).

In this study, we created a recombinant VZV whose capsid protein ORF23 (homolog to VP26) is fused to the green fluorescent protein, as well as the first described VZV dually fluorescent viruses where a tegument protein (ORF9, ORF21 or ORF22, respectively) is additionally fused to a red fluorescent protein. With these viruses, we showed that (i) nuclear structures located at the periphery of the RC are formed during VZV infection; (ii) they appear in all cell types around 8–12 h post-infection, as soon as the RC starts to form; (iii) they contain capsid/procapsid proteins, some but not all tegument proteins, whereas they do not contain proteins associated with DNA replication and encapsidation; (iv) they are not only mainly constituted of fully assembled capsids of the three types, but also many procapsids, as well as a few partial capsids; and (v) they are highly dynamic. We believe that the observed structures might represent a place where capsids are preferentially assembled and/or accumulated after or during their formation, and before their egress towards the cytoplasm.

Results

Construction of an eGFP-ORF23-tagged VZV.

In order to study the nuclear steps of VZV virion assembly, we generated a virus whose minor capsid protein ORF23 (HSV-1 VP26 homolog) is fused to the green fluorescent protein (eGFP). Homologous recombination in *Escherichia coli* was used to modify a BAC containing the entire pOka genome of VZV. In two separate experiments, we inserted the eGFP coding sequence either upstream or downstream of the *orf23* gene (Fig. 1A). The two BACs were transfected in MeWo cells, which were passaged near confluence until typical infection foci appeared. In three successive experiments, transfection of the BAC ORF23-eGFP failed to give rise to infection foci, even four weeks after transfection, whereas transfection of the BAC eGFP-ORF23 led to a productive infection. The growth property of the fluorescently labeled virus was compared with a pOka strain obtained after the transfection of the unmodified BAC-VZV. Even though the recombinant virus is viable and infectious, the expression of a fluorescently tagged ORF23 alters viral growth (Fig. 1B). The expression of the eGFP-fusion protein was verified by western-blotting on total cell extracts of infected MeWo cells with an antibody against GFP (Fig. 1C). The fusion protein is detected as a doublet, slightly higher than expected from the predicted molecular weight (51 kDa). This is consistent with previously published results suggesting that ORF23 might present phosphorylation-dependent isoforms (Chaudhuri et al., 2008).

Intense nuclear fluorescent spots appear in VZV-infected cells

Living MeWo cells asynchronously infected with eGFP-VZV display specific fluorescence patterns characterizing their stage of infection. At early stages, infected cells present arrays of incoming capsids docked at the nuclear membrane (Fig. 2A, cell 1). At the beginning of the late phase of gene expression, ORF23 starts to be produced, which is characterized by a diffuse eGFP signal both in the cytoplasm and the nucleus (Fig. 2A, cell 2). At later stages, the assembly of progeny virions initiates and bright dots corresponding to single capsids show up in the nucleus (Fig. 2A, cell 3), after which very intense larger nuclear fluorescent spots resembling HSV-1 assemblons begin to appear (Fig. 2A, cell 4).

Because HSV-1 assemblons form only in certain cell types and at very late time points (Ward et al., 1996), which casts doubt on their potential role in capsid assembly, we first wanted to evaluate the presence of such nuclear structures in various cell types. Human primary foreskin fibroblasts (HFF) were infected via a 20 min cell contact with eGFP-ORF23-infected MeWo cells, followed by extensive washing, and a coverslip was fixed every hour in a 24 h time frame. The cells were immunostained against beta-tubulin and analyzed by confocal microscopy. Selected time points are presented in Fig. 2B. Incoming capsids docked at the nuclear envelope were observed 3 h p.i. (this stage corresponds to cell 1 in Fig. 2A), but the green diffused fluorescence resulting from *de novo* ORF23 expression only became detectable at around 6 h p.i. (this stage correspond to cell 2 in Fig. 2A). At 8 h p.i., newly assembled capsids appeared throughout the nucleus (like cell 3 in Fig. 2A), sometimes in tiny aggregates. Brighter and larger fluorescence dots, similar to those seen in MeWo cells (cell 4, Fig. 2A), were present from 12 h p.i. and grew in size as the infection progressed (Fig. 2B). In a parallel experiment, time-lapse video imaging was performed and confirmed the successive pattern (1–4) of the green fluorescence as the infection progressed (Movie S1). The brightness of the eGFP enables the detection of single capsids inside infected cells and the analysis of several movies showed that it takes about 3 h from the emergence of the diffused eGFP signal until newly formed capsids show up in the nucleus (a 2 h 30 min time frame separates stages 2 and 3 in Movie S1), and only one more hour until the larger fluorescent spots begin to form (Fig. 2C compare t0+30' and t0+75' or t0+90'). We noticed that the larger fluorescent spots actually appeared before the massive accumulation of capsids in the cytoplasm, where secondary envelopment occurs (Movie S1, cell on the left, Fig. 2C compare t0+75' with t0+4 h 15 or t0+5 h 45 and Movie S2, arrows). Such nuclear dense fluorescent structures also formed in human primary embryonic lung fibroblasts (MRC5) and human keratinocytes immortalized via permanent TERT expression (N/TERT-1) (Fig. 2D). The latter cell line had been shown to maintain most of the characteristics of primary keratinocytes and constituted a model closer to the preferential natural host of the virus. One should also note that similar nuclear dense structures also appeared both with a virus generated in our lab and expressing ORF23 fused to the

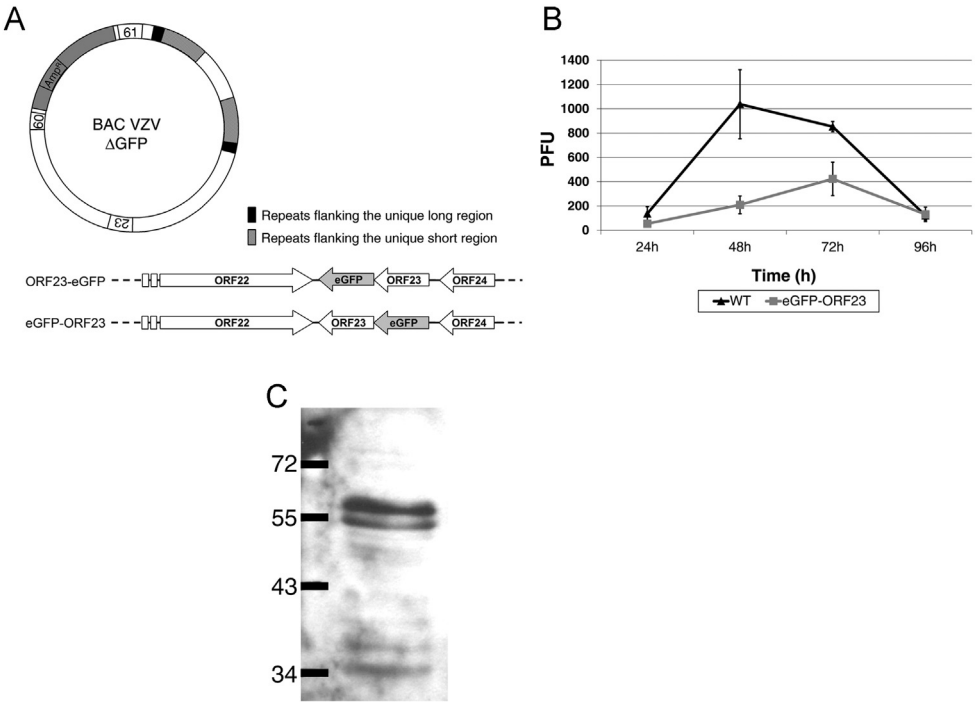

Fig. 1. Creation of an eGFP-ORF23 VZV. (A) Schematic representation of the BAC-VZV ΔGFP and of the genomic region of the two BACs where ORF23 has been fused to eGFP. AmpR, Ampicillin resistance gene; 60, 61 and 23, position of the corresponding ORF within the BAC. (B) Growth curve of the eGFP-ORF23 VZV compared to the pOka parental strain (WT). At day 0, four 25 cm^2 flasks were prepared by mixing 3×10^6 uninfected MeWo cells with 200 VZV infected cells. At the indicated periods of time, the number of plaque forming units (PFU) was assessed as described in the Materials and methods section. Means of a representative experiment out of three are depicted; error bars represent the standard deviation. (C) Western-blotting on total cell extract of MeWo infected with eGFP-ORF23 VZV with an antibody against GFP (expected size of the fusion protein: 51 kDa).

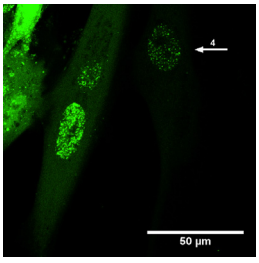

Movie S1. Live imaging of HFF cells infected with eGFP-ORF23. HFF cells were seeded on 35-mm glass bottom dish and infected with eGFP-ORF23 VZV via a 20-min cell contact with MeWo cells. 12h post infection, images were recorded every 15 min over a 13 h time frame using a confocal microscope equipped with a chamber controlling the temperature, as well as the humidity and CO_2 level. Confocal microscope images were captured with a 60 × oil-objective. A video clip is available online. Supplementary material related to this article can be found online at doi:10.1016/j.virol.2014.02.023.

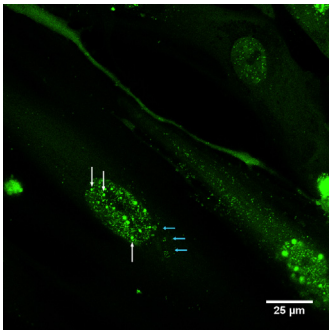

Movie S2. The nuclear dense structures appear prior the massive accumulation of newly formed capsids within the cytoplasm. HFF were infected via cell contact with eGFP-ORF23 MeWo cells. 12h post infection, fields where the cells presented a diffuse cytoplasmic and nuclear signal and few nuclear dots corresponding to individual capsids were selected. Images were recorded every 10 min over a 14 h time frame using a confocal microscope equipped with a chamber controlling the temperature, as well as the humidity and CO_2 level. Confocal microscope images were captured with a 60 × oil-objective. The white arrows point to the nuclear intense fluorescent spots; cyan arrows show the accumulation of capsids within the cytoplasm. A video clip is available online. Supplementary material related to this article can be found online at doi:10.1016/j.virol.2014.02.023.

tagRFP-T, which is a true monomeric red fluorescent protein (Fig. S1A), and in wild-type-VZV-infected cells labeled with an anti-ORF23 antibody (Fig. S1B). The fact that these structures appear very early, before the massive accumulation of capsids in cytoplasmic areas, and their presence in all tested cell lines contrasts with the characteristics described for HSV-1 assemblons, led to our decision to investigate whether they share other features.

VZV induced nuclear dense structures are located at the periphery of the RC and contain the major capsid protein, the procapsid scaffold protein but not the DNA terminase subunit 1

We first wondered whether other viral proteins implicated in the different nuclear steps of virion formation were present in these discrete nuclear compartments.

MRC5 cells were infected by a 20 min contact with eGFP-ORF23 VZV MeWo cells followed by extensive washing. Coverslips were then fixed at 8, 12, 16, 24 and 36 h p.i. and immunostained for ORF29 (the single-strand DNA binding protein, homologous to HSV-1 ICP8), ORF40 (major capsid protein, homologous to HSV-1 VP5), uncleaved ORF33/33.5 (procapsid scaffold protein, homologous to pre-VP21/VP24 and pre-VP22a) and ORF45/42 (DNA packaging terminase, subunit 1, homologous to UL15). Selected time points are presented in Figs. 3 and 4. The expression of ORF29 allowed us to delineate the RC (Fig. 3, dashed line) which started

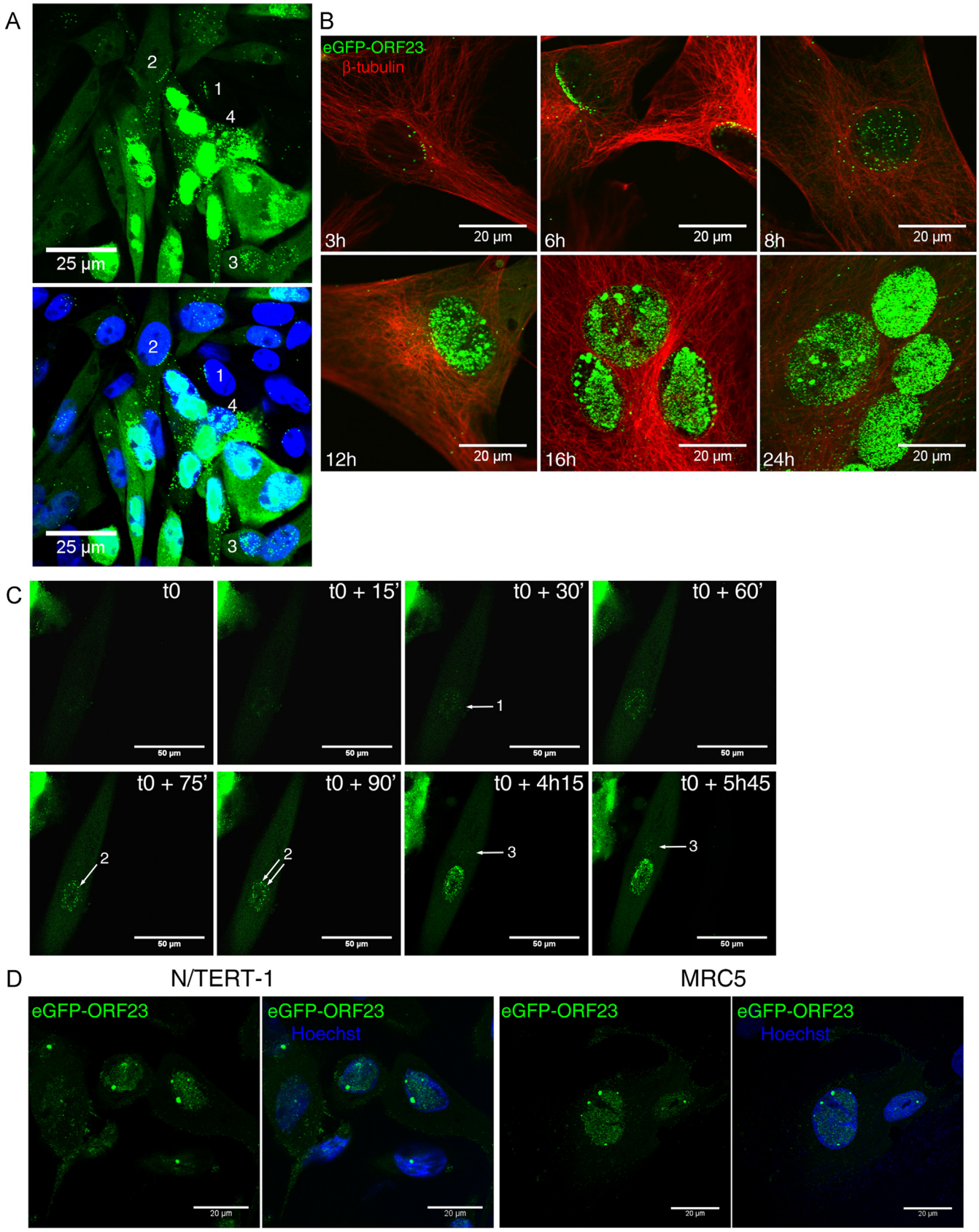

Fig. 2. Nuclear dense structures form in eGFP-ORF23 VZV infected cells. (A) Live visualization of MeWo cells infected for 24 h with eGFP-ORF23 VZV. Nuclei were stained with Hoechst 33342 and confocal microscope images were captured with a 63 × oil-objective. Numbering represents gradual stages of infection. (B) Human primary foreskin fibroblasts (HFF) were infected with eGFP-ORF23 VZV via a 20-minute contact with MeWo cells followed by extensive washing. HFF were fixed at indicated times p.i. and immunostained against beta-tubulin (Alexa568 secondary antibody). (C) Selected frames of a time-lapse experiment of human primary foreskin fibroblasts (HFF) infected with eGFP-ORF23 VZV; white arrows point to the onset of the first newly assembled capsids (1), followed by the emergence of nuclear dense structures (2) and the apparition of capsids in cytoplasmic areas (3). (D) Human primary embryonic lung fibroblasts (MRC5) and human normal keratinocytes immortalized by permanent TERT expression (N/TERT-1) infected with eGFP-ORF23 were fixed 24 h p.i. and nuclei counterstained with Hoechst 33342. Confocal microscope images were captured with a 63 × oil-objective.

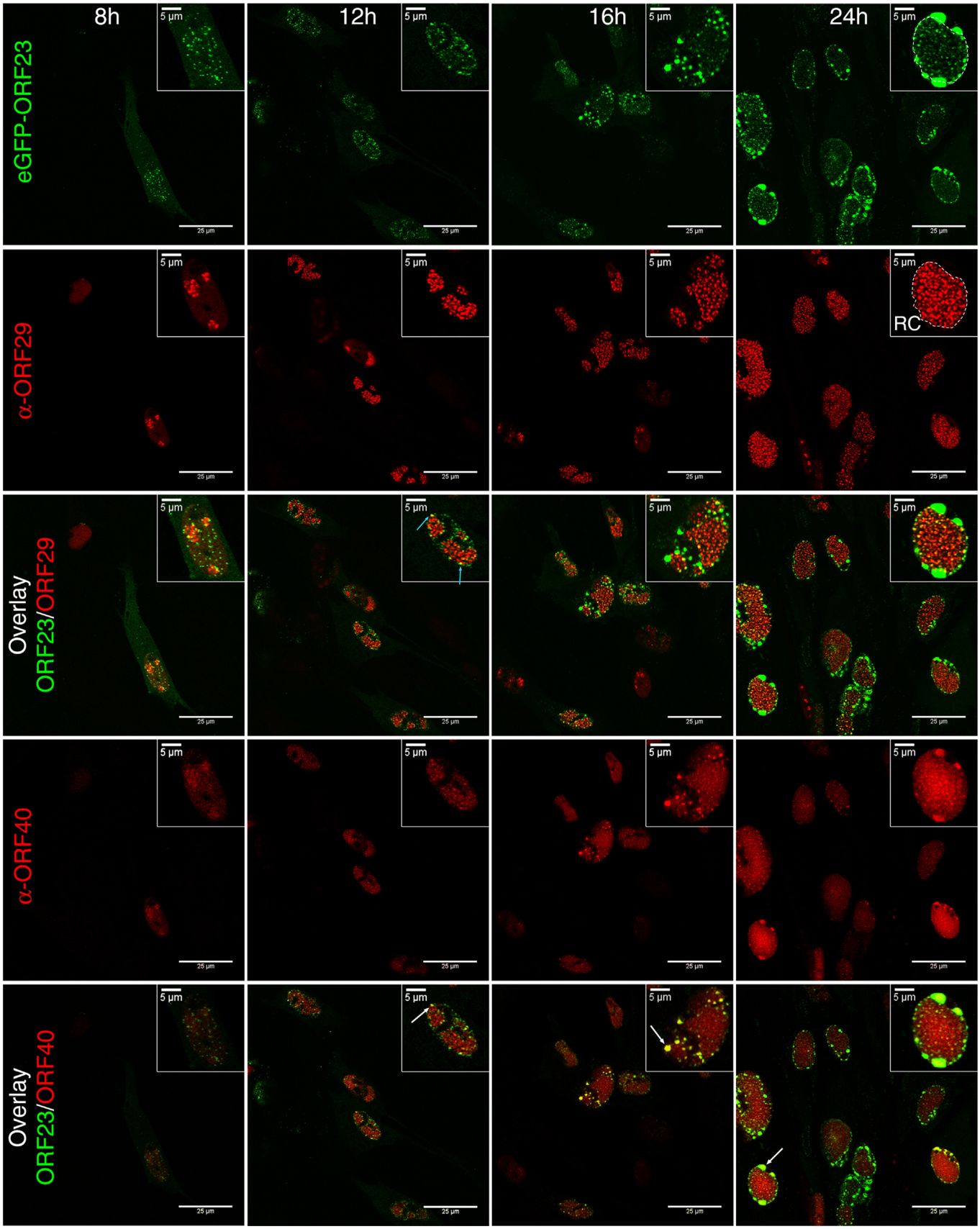

Fig. 3. The nuclear dense structures contain the major capsid protein and partially overlap with ORF29. MRC5 infected with eGFP-ORF23 VZV were fixed at indicated times p.i. and immunostained with both mouse anti-ORF40 and rabbit anti-ORF29 primary antibodies. Alexa568-anti-rabbit and Alexa633-anti-mouse were used as secondary antibodies. Confocal microscope images were captured with a 63 × oil-objective. The ORF29 staining was used to draw the dashed line representing the RC, which was then reported on the eGFP picture. Cyan arrows show partial overlapping between eGFP-ORF23 and ORF29 signals. White arrows point to structures where ORF40 co-localizes with eGFP-ORF23.

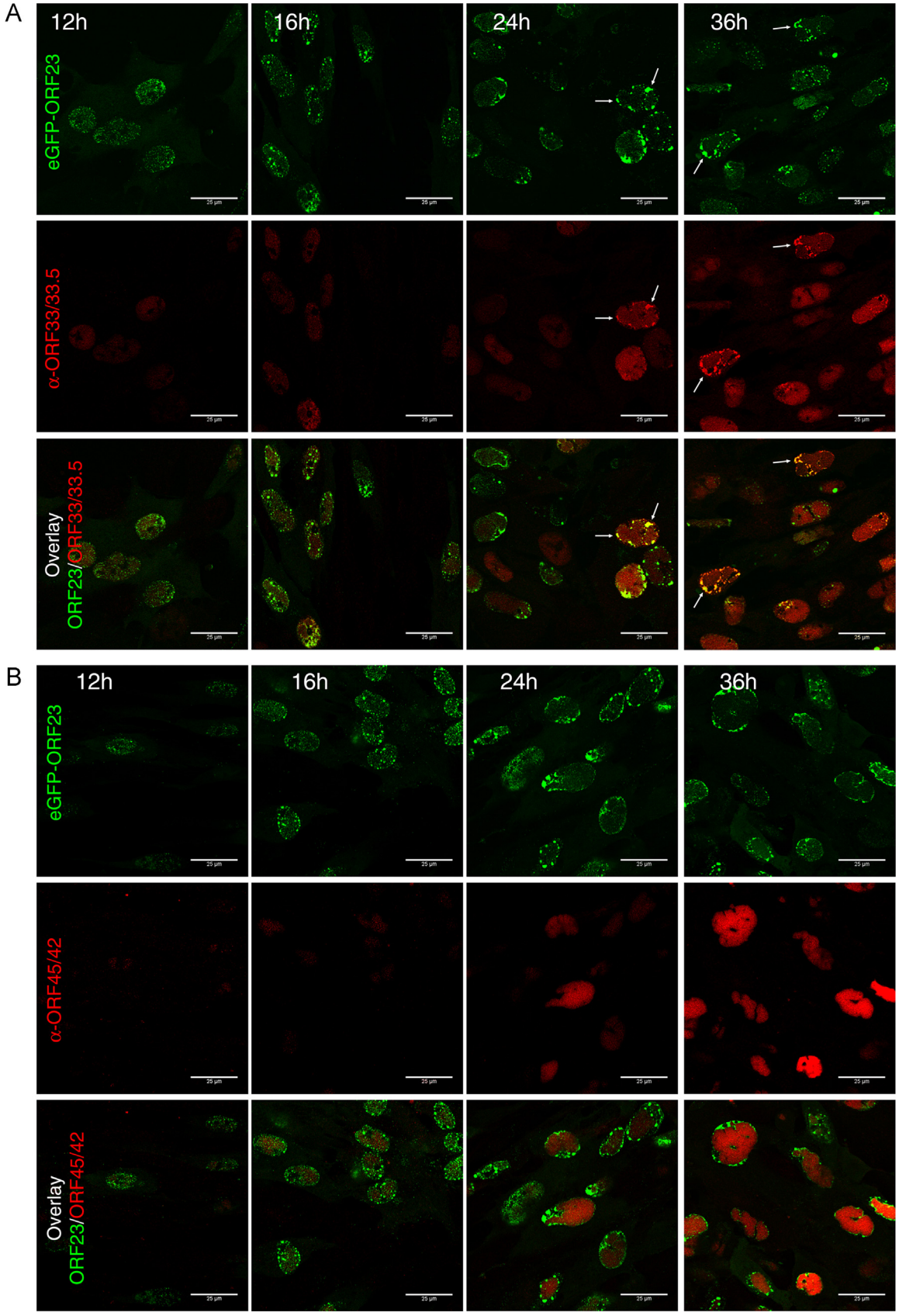

Fig. 4. The procapsid scaffold protein but not the DNA terminase subunit 1 is present in the nuclear dense structures. MRC5 infected with eGFP-ORF23 VZV were fixed at the indicated times p.i. and immunostained with an anti-ORF33/33.5 (scaffold protein and maturing protease) (A) or an anti-ORF45/42 (DNA terminase subunit 1) (B) primary antibody (Alexa568 secondary antibody in both cases). Confocal microscope images were captured with a 63 × oil-objective. White arrows point to co-localization.

to form around 8 h p.i. at several spots that enlarged and fused in a single large area around 24 h p.i. The ORF29 labeling partially overlapped the eGFP signal (Fig. 3, cyan arrows) but the co-localization area remained rather discrete and did not grow with the infection. This suggests that, if there is any, viral DNA replication can only occur in a very small part of this nuclear compartment. Small isolated eGFP-dots corresponding to individual capsids could be found sparsely within, as well as outside, the RC, albeit the vast majority of the eGFP larger spots were located at the periphery of the RC.

The major capsid protein (ORF40) appeared in the nuclear structures at 12 h p.i. and started to strongly accumulate at 16 h p.i (Fig. 3, white arrows), whereas the presence of ORF33/33.5 corresponding to the viral procapsid scaffold was more delayed and was only substantially visible at late time points (24 and 36 h p.i.) and in only certain very large structures (Fig. 4A). On the contrary, the DNA terminase encoded by ORF45/42 never seemed to accumulate in the dense structures (Fig. 4B). We can conclude from these results that, like the HSV-1 assemblons, the observed structures ultimately contain important proteins implicated in capsid assembly but not those proteins that are implicated in DNA replication and encapsidation.

We next wondered whether the structures observed by confocal microscopy would be distinguishable at the ultrastructural level and if they were constituted of fully or partially assembled capsids or of capsid proteins.

The nuclear dense structures are capsid aggregates that grow in size in the course of the infection

In order to precisely and irrefutably characterize the nature of the nuclear dense structures observed in confocal microscopy, we decided to carry out correlative microscopy. MeWo cells were grown on a glass-bottom dish, infected for 48 h with eGFP-ORF23 VZV, fixed with paraformaldehyde, stained with Hoechst and analyzed by confocal microscopy. A Z-stack image was recorded for each infection focus present on the glass coverslip that was then unglued from the plastic dish via a short contact with methanol. The cells on the coverslip were fixed again with glutaraldhehyde and osmium tetroxide, embedded in epon and processed for transmission electron microscopy (TEM). Ultrathin sections were carefully examined and compared with confocal images to clearly assess a concordance. Pictures of the chosen area were then systematically recorded on all available sections. The image of an infection focus was reconstructed from ten separate TEM images (Fig. 5A) and compared with the confocal Z-stack and (Fig. 5B). As seen on the higher magnifications (Fig. 5C and D), each intense fluorescent spot, regardless of its size, corresponds, at the ultrastructural level to an array of capsids, residing at the periphery of the RC. The latter was easily detectable as a paler area in the center of the nucleus. We confirmed that the size of the capsid aggregates increases over the time during the infection process by analyzing ultrathin sections of MeWo cells infected at 8 h, 12 h, 16 h and 24 h p.i. (data not shown). In order to prove that the dense fluorescence structures observed in wild-type VZV-infected cells immunostained for both ORF23 and ORF40 (Fig. S1) truly reflect the presence of capsid aggregates in a wild-type infection, pOka VZV-infected MeWo cells were analyzed by TEM in parallel of eGFP-ORF23 VZV-infected cells. We indeed detected similar capsid aggregates with the wild-type virus (Fig. 6A). We examined the capsid content of two separate nuclear compartments: the capsid aggregates and the RC. For the latter, we only kept nuclei for which a well-defined RC was present and to avoid bias due to small capsid aggregates and tangent sections of large capsid aggregates, which were present at the periphery of the RC, we excluded a 0.5 μM strip at the edge of the RC from the counting. Over 3000 capsids were counted (within 22 nuclei and 43 capsid aggregates of eGFP-ORF23 VZV-infected cells and 12 nuclei and 14 capsid aggregates for the wild-type infection). We also frequently observed a fourth type of capsid within the aggregates. These particles comprised an inside ring surrounded by a thinner and more defined outer edge and corresponded, by comparison to what is known about HSV-1 (Newcomb et al., 2000; Thomsen et al., 1995), to VZV procapsids (Fig. 6A). For both viruses, we found that the mean percentage of each type of capsid within the aggregates was statistically different from that within the RC. We noted that the predominant form of capsid found within the aggregates is the B type, which is also the most abundant throughout the nucleus. Importantly, capsid aggregates were also enriched in procapsids, which were even totally absent from the central part of the RC in a wild-type infection (Fig. 6B).

During this analysis, we noticed that the distribution of C capsids within the aggregates did not seem random. We then decided to classify them regarding to their position within the aggregates. C capsids that were part of the most exterior layer of capsids were considered as belonging to the periphery. Based on this criteria, we observed that 86% of C capsids within the aggregates actually resided at the periphery (Fig. 6C). If we considered the periphery as the two most external layers of capsid, this percentage peaked to over 95% (data not shown). Another very interesting point was the presence of some partial capsids that were not observed elsewhere in the infected nuclei (Fig. 6D) and which are thought to be precursors of procapsids.

Some capsid aggregates entrapped within PML-cages have recently been described in VZV-infected cells at late time points (Reichelt et al., 2011). We therefore wondered whether the observed structures could represent earlier stages of those aggregates.

VZV nuclear capsid aggregates form independently of the presence of the PML bodies

We generated a MeWo cell line stably expressing a shRNA against all PML isoforms via retroviral vectors particles transductions and from an already described plasmid (pSuper-Retro-Hygro-shPML, a kind gift from Dr. C. Kyratsous; Kyratsous et al., 2009). Non-transduced MeWo cells in parallel with sh-PML expressing cells were infected with eGFP-ORF23 VZV and fixed 24 h p.i. Immunostaining against PML was performed to control the knockdown of the gene (Fig. 7). Nuclear dense fluorescent structures were present in both cell lines showing that the PML bodies are not required for their formation. TEM analysis of eGFP-ORF23 infected-sh-PML MeWo cells revealed the presence of capsid aggregates similar to those observed in non-transduced MeWo cells (data not shown). This suggests that they may represent a virus-induced nuclear compartment that is important for its life cycle rather than a cellular defense that progressively entraps newly formed capsids, impeding their egress. This prompted us to characterize the dynamics of the formation of these structures.

Capsid aggregates are dynamic rather than static structures

We infected MRC5 cells via cell contact with eGFP-ORF23 VZV-infected MeWo cells for 12 h and then took pictures every 2 s over a 15 min time frame (Movie S3). Most of the capsids were in constant movement but a few static fluorescent dots could also be observed. During the 15 min time frame, some of those static dots developed into nascent aggregates whose size constantly evolved whilst seemingly preserving their initial nuclear location (supplemental Movie S3, white arrow). Isolated capsids seemed to constantly move from and towards the aggregates. We next studied the dynamics inside the aggregates via a Fluorescence Recovery After Photobleaching (FRAP) experiment. Infected MRC5

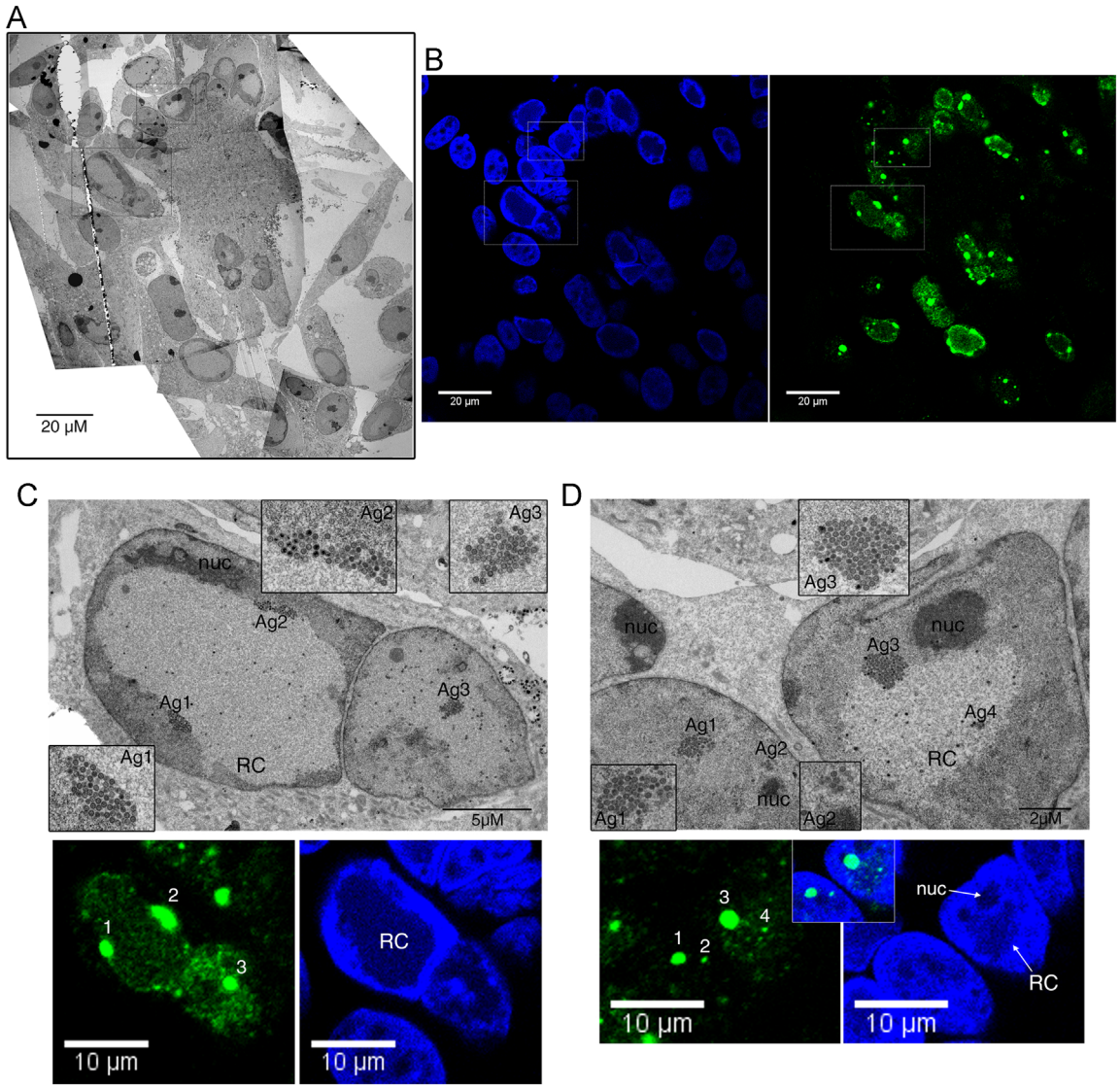

Fig. 5. The nuclear dense structures are capsid aggregates. MeWo cells were infected for 48 h with eGFP-ORF23 VZV in a glass-bottom dish. Cells were fixed, labeled with Hoechst and analyzed by confocal microscopy. A Z-stack of pictures was recorded for each infection focus. The glass coverslip was then separated from the plastic dish and the cell monolayer was re-fixed and embedded in Epon for analysis by Transmission Electron Microscopy. Several pictures obtained by TEM (A) were merged to reconstitute one of the infection focus identified by confocal microscopy (B); dotted line frames delineate areas chosen for the panels C and D. (C) and (D) Higher magnification of field portions: Ag, capsid aggregates (numbered to make the correspondence between TEM and confocal images); nuc, nucleolus; RC, replication compartment.

were analyzed 16 h p.i. in order to obtain aggregates of moderate size. We bleached a region of interest (ROI) corresponding to half of the aggregate during 45 s (Fig. 8 A and supplemental Movie S4) and then took pictures every 15 s. After 2 min post-bleaching, the fluorescence already started to reappear in the bleached area, but it took 10–15 min to return to the original situation where the fluorescence was homogenous overall the entire structure. This speed of fluorescence recovery was not compatible with a fast protein diffusion, like that observed if we bleached a ROI of diffused eGFP in the cytoplasm corresponding to the signal of the fusion protein rather than fully assembled capsid (data not shown). On the contrary, it could be compatible with a movement of capsids within the aggregates, which is expected to be much slower. As there appeared to be a permanent exchange between the capsids residing inside and outside the aggregate (supplemental Movie S3), we performed a Fluorescence Loss In Photobleaching (FLIP) experiment and showed that if the structure was bleached constantly for a certain time, an entire area of the nucleus was bleached (Fig. 8B and supplemental Movie S5). One should note that around 16 h p.i., the RC was very frequently still divided into several areas separated by a thin layer of cellular genomic DNA and each of these replication sub-compartments contained one to three capsid aggregates. Interestingly, supplemental Movie S6 suggested that the capsid aggregates could sometimes give rise to a massive simultaneous transfer of a large amount of capsids from the nucleus to the cytoplasm (see white arrows). Further experiments would be required in order to evaluate the importance of this phenomenon for the VZV lytic cycle and to determine whether this massive transfer occurs via a budding through the inner nuclear membrane or via a transient enlargement of the nuclear pores.

As we hypothesized that not only capsid assembly but also maturation can occur in the described structures, we wondered whether a partial tegumentation could take place there.

The tegument proteins ORF21 and ORF22 but not ORF9 co-localize with the capsid aggregates

Until very recently (Lenac Rovis et al., 2013), antibodies against VZV proteins, in particular against structural proteins, were quite

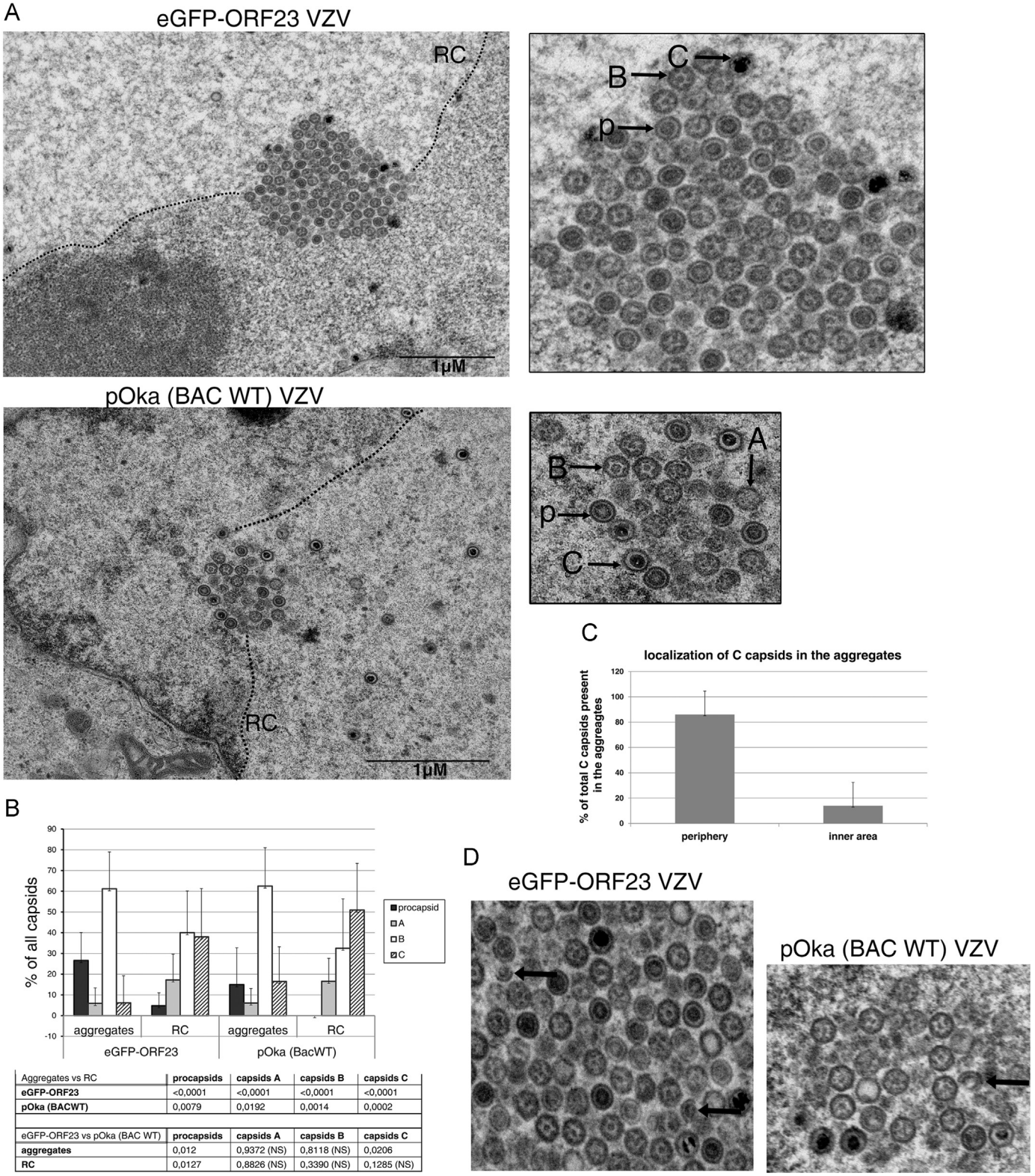

Aggregates vs RC	procapsids	capsids A	capsids B	capsids C
eGFP-ORF23	<0,0001	<0,0001	<0,0001	<0,0001
pOka (BACWT)	0,0079	0,0192	0,0014	0,0002

eGFP-ORF23 vs pOka (BAC WT)	procapsids	capsids A	capsids B	capsids C
aggregates	0,012	0,9372 (NS)	0,8118 (NS)	0,0206
RC	0,0127	0,8826 (NS)	0,3390 (NS)	0,1285 (NS)

Fig. 6. Nuclear capsid aggregates present a characteristic organization and contain many procapsids. MeWo cells infected with eGFP-ORF23 or pOka VZV were analyzed by TEM. The proportion of the four types of capsids (procapsids, A, B and C, black arrows) present within the aggregates and the replication compartment was determined by systematic counting of randomly chosen infected nuclei. Representative pictures are shown in (A) and mean percentages in (B); error bars represent the standard deviation. Mean percentages were pairwise compared using a two-tailed t-test in order to determine statistically significant differences; *p* values are presented in the table under the graph, NS, non-significant. (C) The C capsids present within the aggregates were divided into two categories on the basis of their localization; periphery was strictly determined as the most exterior layer of capsids and mean percentage are shown, with error bars representing the standard deviation. (D) Late partial capsids can be found in the nuclear capsid aggregates of both viruses (black arrows).

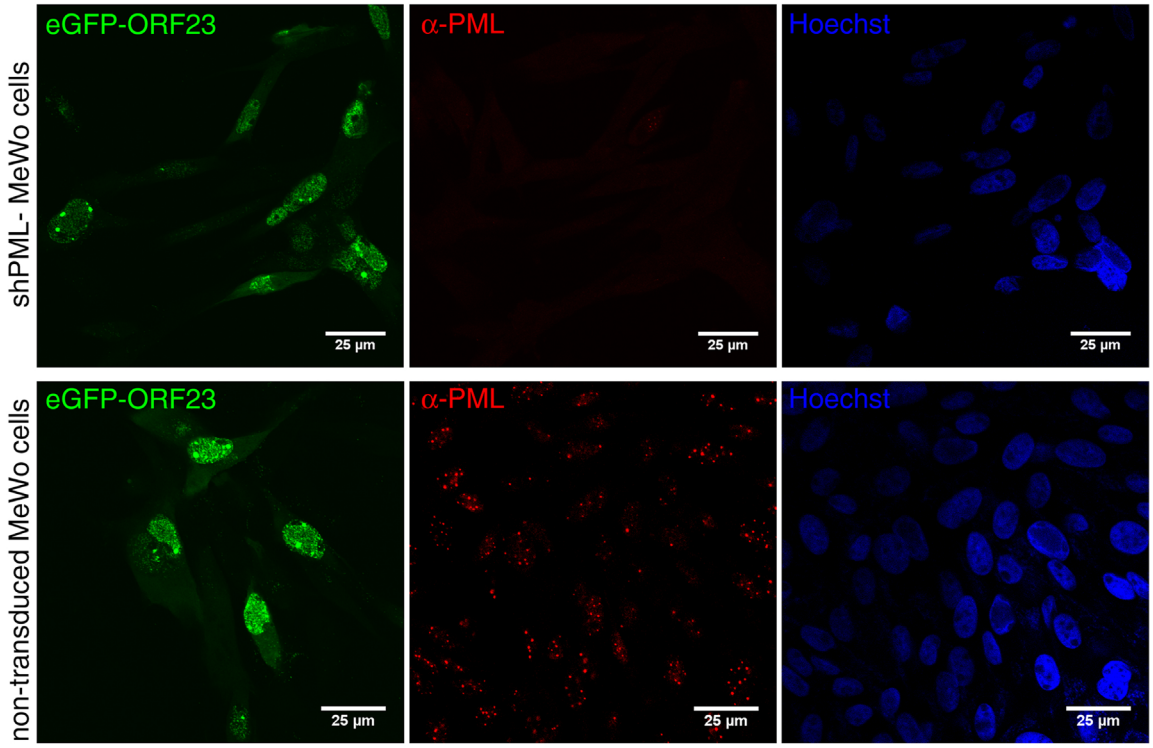

Fig. 7. The nuclear dense structures corresponding to capsid aggregates also appear in PML-depleted cells. shPML-MeWo cells as well as non-transduced MeWo cells were infected with eGFP-ORF23 VZV for 24 h and analyzed by immunofluorescence using an anti-PML antibody (Alexa568 secondary antibody). Confocal microscope images were captured with a 63 × oil-objective.

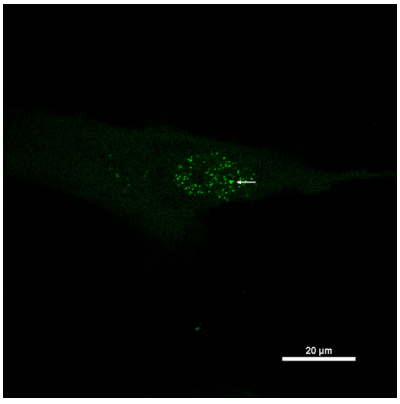

Movie S3. Nuclear capsid aggregates are dynamic structures that seem to originate at specific locations. MRC5 were infected via cell contact with eGFP-ORF23 MeWo cells. 12h post infection, pictures were recorded every 2 s for a 15 min period. Confocal microscope images were captured with a 60 × oil-objective. White arrow points to the nascent aggregate. A video clip is available online. Supplementary material related to this article can be found online at doi:10.1016/j.virol.2014.02.023.

sparse and were not always suitable for immunostaining. In order to identify potential tegument proteins residing in the structures, dually fluorescent VZV were created, starting from our eGFP-ORF23 BAC construct. Three different proteins were chosen: ORF21 and ORF22, homologous to HSV-1 UL37 and UL36, respectively, which are supposed to belong to the inner tegument, and ORF9, corresponding to HSV-1 VP22. As we had already determined from the targeting of ORF23 that the orientation of the fluorescent tag regarding the gene could be of a great importance, we directly tested both possibilities. Moreover, in order to maximize our chances of obtaining viable viruses with the brightest fusion protein, two different red fluorescent tags were used: DsRed-monomer (referred to as "mDsRed") and tagRFP-T (referred to as "tRFP-T"). Only three of the 12 different BACs that were created gave rise to highly infectious VZV after transfection into MeWo cells (Fig. 9A). Other constructs either totally failed to lead to infection foci, even four weeks after transfection, or engendered very slowly replicating viruses (data not shown). The addition of a second fluorescent tag did not seem to further impact the replication kinetics of the virus (Fig. 9B). The distribution of the red fluorescence in infected living MeWo cells (Fig. 9C) 24 h p.i. revealed that the three proteins were present mostly in the cytoplasm, but also in some discrete nuclear locations. ORF21 and ORF22 were present in some of the capsid aggregates (Fig. 9C, white arrows), although, most of the time, only a portion of the eGFP-ORF23 area was also positive for either mDsRed-ORF21 or mDsRed-ORF22 (Fig. 9C, insets). On the contrary, ORF9, which was mostly displayed as cytoplasmic aggregates, was never detected in these nuclear structures.

Discussion

The entire process of VZV virion formation and egress is far from being fully elucidated. Nucleocapsid formation in the infected cells leads to dramatic changes in the nuclear architecture, the role of which is not entirely understood.

In order to better understand these processes, we created a virus with the small capsid protein ORF23 fused to the eGFP. With this virus, we identified nuclear fluorescent dense structures emerging around 8–12 h p.i. and enlarging whilst the infection progressed. As revealed by confocal microscopy, the identified structures contain capsid and procapsid proteins as well as some proteins that supposedly belong to the inner tegument. This prompted us to question whether they were similar to the already described HSV-1 assemblons. These structures were first identified in optical microscopy with antibodies against capsid proteins, but the fusion of HSV-1 VP26 with different fluorescent tags has

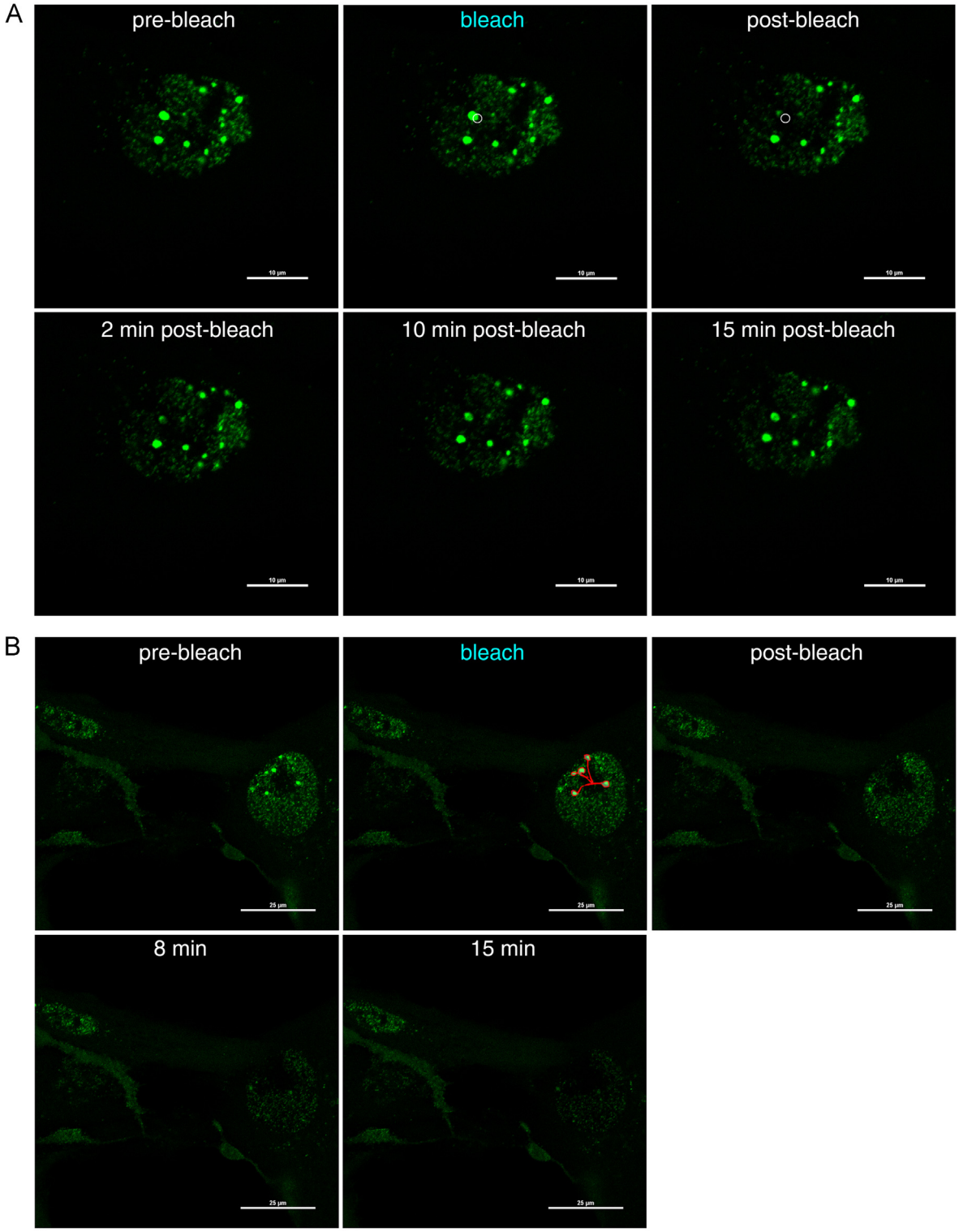

Fig. 8. Nuclear capsid aggregates are dynamic structures. MRC5 cells were infected for 16 h with eGFP-ORF23 VZV via cell contact followed by extensive washing. (A) A region of interest (ROI) represented by the white circle was bleached for 45 s and then an image was recorded every 15 s for 15 min. Selected time points are shown. (B) A ROI represented by the red shape was first bleached for 1 min before successive steps of bleaching and image acquisition. Selected time points are shown. Confocal microscope images were captured with a 60× oil-objective equipped with a chamber controlling the temperature and the CO_2 level.

demonstrated that this protein forms peculiar aggregates whose size increases during the course of the infection and likely correspond to the assemblons (de Oliveira et al., 2008; Desai and Person, 1998). Remarkably, the C-terminal region of VP26 containing stretches of conserved residues has been demonstrated to carry an interaction motif with the capsids and to redirect VP26 to nuclear spots defined as assembly sites (Desai et al., 2003). Nevertheless, attempts to relate those intense fluorescent spots with some virus-induced structures, discernible on ultrathin sections of infected cells, have remained quite scarce (Feierbach et al., 2006; Nagel et al., 2012). A recent publication has even shown that the fusion of HSV-1 VP26 with some fluorescent tags can lead to

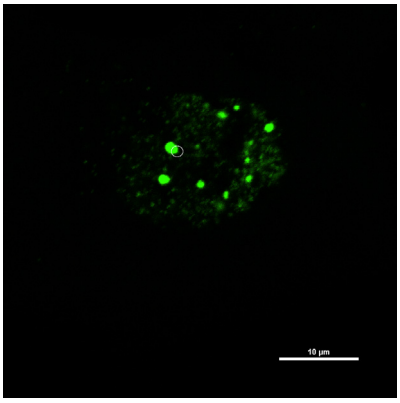

Movie S4. FRAP experiment showing that capsids within the nuclear aggregates are not static. MRC5 were infected via cell contact with eGFP-ORF23 MeWo cells. 16h post infection, a region of interest represented by the white circle, was bleached for 45 s and then an image was recorded every 15 s for 15 min. Confocal microscope images were captured with a 60× oil-objective. A video clip is available online. Supplementary material related to this article can be found online at doi:10.1016/j.virol.2014.02.023.

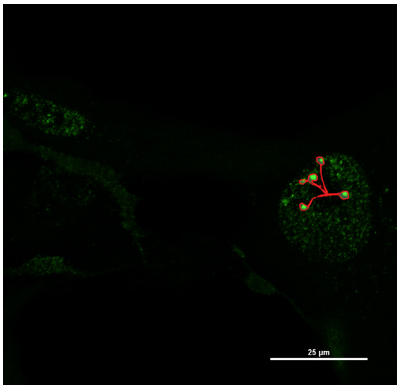

Movie S5. FLIP experiment showing that capsids are constantly moving from and towards the nuclear aggregates. MRC5 were infected via cell contact with eGFP-ORF23 MeWo cells. 16h post infection, a region of interest represented by the red shape, was first bleached for 1 min before successive steps of bleaching and image acquisition. A video clip is available online. Supplementary material related to this article can be found online at doi:10.1016/j.virol.2014.02.023.

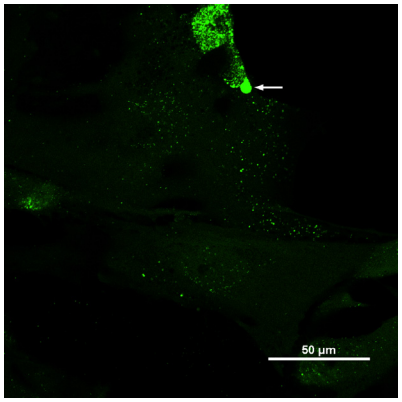

Movie S6. Entire capsid aggregates seem to be able to be transferred into the cytoplasm in one step. HFF were infected via cell contact with eGFP-ORF23 MeWo cells. 16h post infection, pictures were recorded every 15 min over a 13 h time frame. White arrows show two successive bursts of capsid aggregates within the cytoplasm. A video clip is available online. Supplementary material related to this article can be found online at doi:10.1016/j.virol.2014.02.023.

the formation of fusion protein aggregates impeding viral growth (Nagel et al., 2012). Here, in VZV-infected MeWo cells, we show indisputably, via correlative microscopy, that the nuclear structures observed in confocal microscopy actually correspond to capsid aggregates identified in electron microscopy. We compared our eGFP-ORF23 VZV with a wild-type virus, and observed similar nuclear dense structures in confocal microscopy corresponding to similar capsid aggregates found in TEM. This proves that the structures described here were not artefactually induced by the eGFP-ORF23 fusion protein. Even though we cannot exclude the possibility that VZV behaves differently from the other alphaherpesviruses, we believe that it might be very important to reevaluate some HSV-1 and PRV data, in light of the current study.

The major question to be asked concerns the potential functionality of these nuclear structures. The presence of numerous A, B and C capsids, as well as many procapsids, suggests that they may indeed represent sites where assembly can take place. Procapsids are usually rarely seen in the nucleus of infected cells, due to their rapid maturation into A, B and C capsids (Newcomb et al., 1996; Trus et al., 1996). The high percentage of procapsids within the aggregates, and the identification, only in this nuclear compartment, of partial procapsids, representing earlier stages of assembly (Newcomb et al., 1999), are strong arguments in favor of a functional role of these structures. Of course, these sites are highly unlikely to be the sole location of capsid formation, since some infected nuclei are devoid of them and the first newly formed capsids appear randomly distributed within the RC. Of note, while procapsids are completely absent from the RC in a wild-type infection, a significant amount of them can be found in the RC of cells infected with the eGFP-ORF23 VZV. Moreover, the proportion of procapsids within the aggregates is significantly higher for the eGFP-ORF23 compared to the wild-type virus (26.6% vs. 14.9%). We believe that this may reflect a slower maturation rate, probably due to the presence of the eGFP tag, and this could, in part, explain the growth defect of the recombinant virus compared to the wild-type. The presence of the tag could, for example, impact the assembly of the portal complex or the expulsion of the scaffold. This could explain the negative dominant effect observed with some fluorescent protein-VP26 fusion combinations, which were described for HSV-1(Nagel et al., 2012) and that we actually observed in an attempt to fuse ORF23 to mCFP and mYFP (data not shown). If true, the fact that we observed a few procapsids within the RC of eGFP-ORF23 VZV-infected nuclei suggest that, indeed, a few number of capsids are produced in this nuclear compartment but that the procapsids are very rapidly converted in ulterior maturation stages, rendering their visualization quite difficult in a wild-type infection.

Another interesting point is that the capsids within the aggregates are not organized randomly. C-capsids are almost always found at their periphery, and, also, the proportion of the different types of capsids does not mirror that found in the rest of the nucleus. If the aggregates were simply due to an excess of capsids at late time points of infection, these observations would not be expected. It is tempting to speculate that DNA encapsidation occurs at the periphery of the aggregates, but our data cannot exclude the possibility that some C capsids produced in the RC could later be sequestered at the periphery of these aggregates.

The presence of numerous B capsids, which are largely thought to be dead end particles, in the aggregates surely provides an argument for a depot of mostly immature capsids with no function in the viral life cycle. It would be very interesting to measure the proportion of the different types of capsid within the aggregates over time to evaluate whether their increasing size is mainly attributable to an increasing number of B capsids.

Some VZV capsid aggregates entrapped in PML-cages have recently been identified in the nucleus of infected cells (Reichelt et al., 2012; Reichelt et al., 2011), which is believed to limit capsid egress to the cytoplasm. We first thought that the structures described here represented earlier stages of this phenomenon.

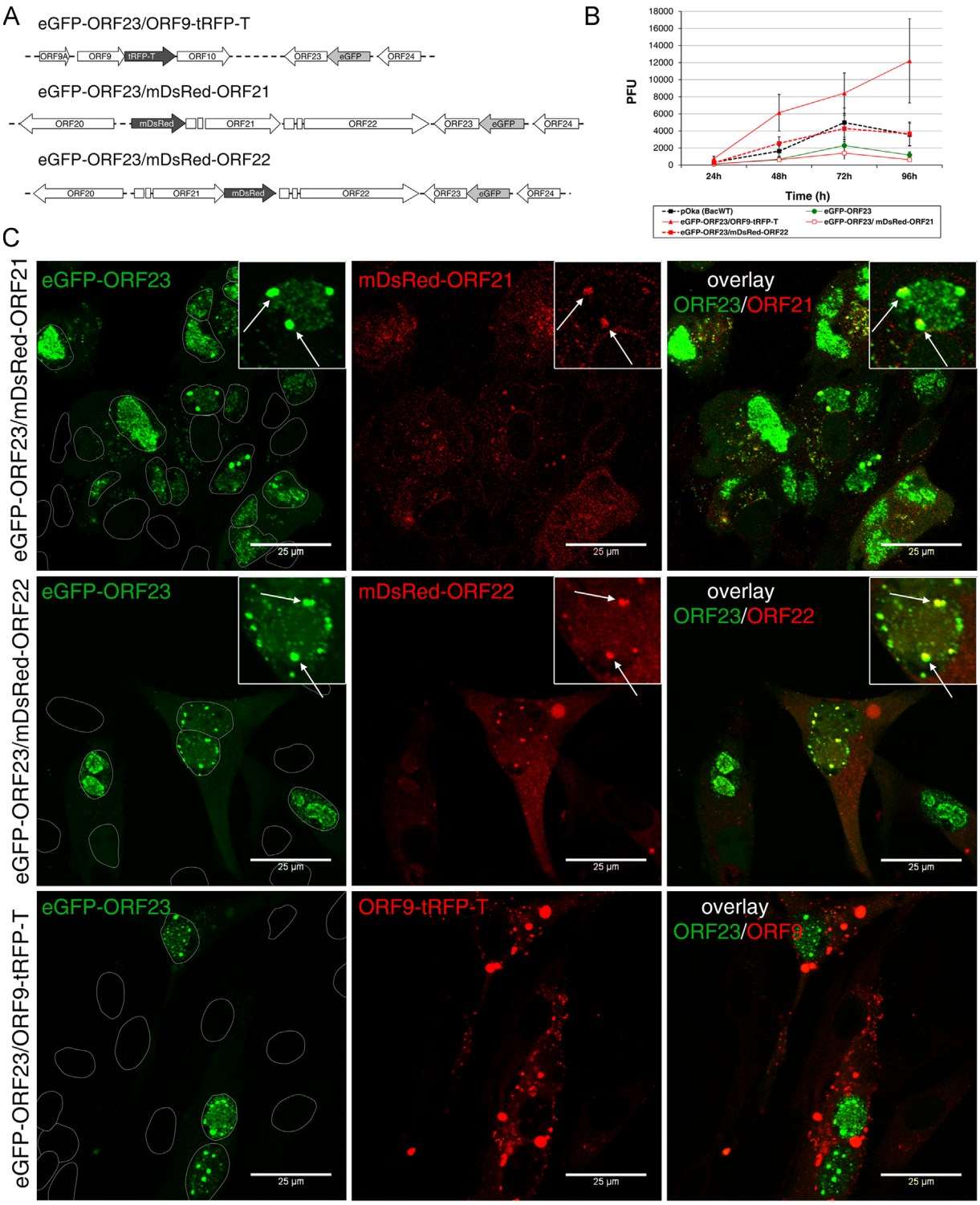

Fig. 9. ORF21 and ORF22 tegument proteins co-localize with nuclear capsid aggregates whereas ORF9 does not. (A) Schematic representation of the genomic region that has been modified in the BAC-VZV eGFP-ORF23 to create the dually fluorescent viruses. (B) Growth curve of the dually fluorescent viruses compared to the eGFP-ORF23. The same technique was used as described in Fig. 1A, except that 500 infected cells were used instead of 200. Means of a representative experiment out of three are depicted; error bars represent the standard deviation. (C) Live visualization of MeWo cells infected for 24 h with eGFP-ORF23/mDsRed-ORF21, eGFP-OR23/mDsRed-ORF22 or eGFP-ORF23/ORF9-tRFP-T. Nuclei were labeled with Hoechst and confocal microscope images were captured with a 63× oil-objective. White arrows in insets point to co-localization between eGFP-ORF23p and mDsRed-ORF21 or mDsRed-ORF22; solid grey lines delineate nuclei from the Hoechst labeling.

However, when we silenced PML gene expression via shRNA technology, we still observed eGFP-ORF23 intense fluorescent spots in confocal microscopy, as well as capsid aggregates in TEM (data not shown). Moreover, we demonstrated, by FRAP and FLIP technology, that there is a constant movement of capsids within the structures as well as a permanent exchange between the capsids residing in the structures and the capsids present elsewhere in the replication sub-compartments. Of note, an interesting study on PRV showed that the formation of capsid assembly sites within the nucleus is a dynamic process requiring a

virally induced "nucleo-squeleton" (Feierbach et al., 2006). We cannot exclude the possibility that the dynamic nature and the growing size of the aggregates could also reflect an inability of the capsids to efficiently egress the nucleus towards the cytoplasm. In that case, aggregates could then be locations where capsids simply accumulate, maybe in order to gain some of the properties that are necessary for the future egress or simply waiting for some processes to be achieved, like the disruption of the nuclear lamina or the maturation of the RC, subsequently giving the capsids access to the inner nuclear membrane through which they need to bud.

The ultimate demonstration that the structures identified here have a crucial role for the virus life cycle would require a system in which we can impede their formation and show that it impacts capsid formation or egress, which is, unfortunately, difficult to set up. Nevertheless, attempts to prove that the nuclear punctuated patterning of VP26 is essential for viral replication have recently been carried out on EBV and KSHV with capsid self-assembly systems. Indeed, VP26 nuclear distribution has been shown to be dependent on its interaction with the major capsid protein and the deletion of the region that is essential for its peculiar localization in the nucleus impedes capsid formation (Henson et al., 2009; Perkins et al., 2008).

In this study, we created the three first dually fluorescent VZV where, not only ORF23, but also an additional tegument protein was fluorescently labeled.

With these viruses, we showed that ORF9 is mainly displayed as cytoplasmic aggregates that could be related to its role in secondary envelopment which we recently demonstrated (Riva et al., 2013). The localization of ORF21 and ORF22, belonging to the inner tegument, in the nuclear capsid aggregates revives the debate surrounding where the initial step of tegumentation takes place. The presence of UL36 (ORF22 homolog) in the nucleus of PRV and HSV-1-infected cells is highly controversial. Some reports demonstrating its presence in the nuclear compartment (McNabb and Courtney, 1992), at the nuclear envelope (Morrison et al., 1998) and its association with intranuclear C capsids (Bucks et al., 2007) are corroborated by the presence in its N-terminal region of a recently described functional and highly conserved, Nuclear Localization Signal (Abaitua and O'Hare, 2008). Moreover, another highly conserved 62 bp sequence, in the C-terminal region of PRV UL36, has been shown to be essential for viral replication and to be able to redirect the GFP to nuclear assemblons upon infection (Lee et al., 2006). This region has since been shown to be functionally conserved in HSV-1 (Coller et al., 2007). On the other hand, some groups failed to detect any UL36 in the nuclear compartment or in association with nuclear capsids, either on ultrathin sections or after extraction on sedimentation gradients (Klupp et al., 2002; Mohl et al., 2009; Trus et al., 2007). The amount of ORF22 found in VZV-infected nuclei is very low compared to the cytoplasmic level and the use of a virus expressing fluorescently tagged ORF22 circumvents issues linked to antibodies' sensitivity and the possible masking of epitopes, potentially through protein conformation or post-translational modifications. This might, in part, explain the discrepancies between some published data and those reported here, bearing in mind that the VZV ORF22 localization has never been specifically investigated before. ORF21 has already been shown in the nucleus of VZV-infected cells, but not in association with peculiar structures (Cohrs et al., 2002). It is very interesting to note that the previously described UL37-GFP/VP26-mRFP-expressing HSV-1 displays a high degree of co-localization of capsids with UL37 at the Trans-Golgi Network, but also at some particular nuclear sites that strongly resemble the structures that we observed (Desai et al., 2008). The localization of both ORF22 and ORF21 at the nuclear capsid aggregates is also corroborated by a very recent report demonstrating that up to 5 tegument proteins could be added to the HSV-1 particle at the nuclear stage, among which were UL36 and UL37 (Henaff et al., 2013). In order to confirm that the addition of a fluorescent tag on both proteins does not alter their localization, we purified VZV virions via two successive gradient steps (sucrose, then potassium tartrate-glycerol) (Kinchington et al., 1995), and, via western-blotting with an antibody against dsRed, confirmed the presence of DsRed-ORF21 in the viral particles (data not shown). However, we were unable to detect the presence of DsRed-ORF22, neither on the infected cell extracts, nor with highly purified virions extracts (data not shown).

A recent Yeast-Two-Hybrid screen has identified ORF21 as an interacting partner of both ORF23 and ORF22 (Stellberger et al., 2010) and HSV-1 and PRV UL36 and UL37 are also well known to interact (Kelly et al., 2012; Klupp et al., 2002; Lee et al., 2008). These interactions could explain the presence of the two tegument proteins in the observed structures.

Of interest, while both UL36 and UL37 of PRV and HSV-1 have been shown to play a role in the viral particle maturation at the cytoplasmic step, PRV UL36 and HSV-1 UL37 specifically have also been shown to be crucial for the nuclear egress (Desai et al., 2001; Desai, 2000; Klupp et al., 2001; Luxton et al., 2006). It is therefore possible that a layer of tegument is necessary for the capsid to bud through the inner nuclear membrane.

To date, we do not know why the co-localization of those two tegument proteins is not homogenous within the capsid aggregates and only arise in some of them, but, as revealed by TEM, the capsid content seemed to evolve during the infection process; it is therefore possible that the protein composition is not homogenous between aggregates. Now that a new bank of antibodies against VZV proteins has been generated (Lenac Rovis et al., 2013), it would, of course, be very interesting to define the protein composition along with capsid type proportions of the structures over time in more detail by using both TEM and confocal microscopy.

Altogether, our data show that VZV induces the formation of nuclear structures containing capsid and tegument proteins, as well as assembled A, B and C capsids and procapsids. These dynamic capsid piles start to appear at specific and defined locations within the nucleus as early as 8–12 h post-infection and are located at the periphery of the replication compartment. We believe that those structures could be implicated in capsid assembly and/or maturation before egress towards the cytoplasm. The presence of two inner tegument proteins suggests that a first step of tegumentation might take place in this nuclear sub-compartment.

Materials and methods

Construction of the BAC-VZVΔGFP

The GFP cassette was removed from the BAC-VZV (kindly provided by Dr. Zhu) and replaced by an ampicillin resistance gene, amplified by PCR with the primers listed in Table S1, via homologous recombination with the *E. coli* strain DY380 according to the recombineering protocol #1 of Dr. Warming at NCI-Frederick. Recombinants were analyzed by PCR and sequencing (Table S2).

Construction of recombinant viruses

Viruses presenting one (or two) open reading frame(s) fused with fluorescent protein encoding genes were constructed by modifying the BAC-VZV-ΔGFP. They were created by bacterial recombineering using the GalK positive/negative selection technique described by Warming et al. (2005) and materials(plasmid pGalK and bacterial strain SW102) were obtained from the Biology Research Branch (BRB) at the NCI, Bethesda, MD. Recombination cassettes were PCR amplified with the specific primers and

templates (Table S1). Recombinants were screened by PCR using the primers listed in Table S2. The constructions were verified by restriction digestion pattern and DNA sequencing.

Cell culture

Human melanoma cell line (MeWo) (ATCC number HTB-65) and human primary embryonic lung fibroblasts (MRC5) were cultured in Eagle's minimal essential medium supplemented with 1% of non-essential amino acids, 1% glutamine, 1% antibiotic mix (penicillin–streptomycin) and 10% FBS (Fisher Scientifics, GIBCO). Primary Human Foreskin Fibroblasts (HFF) were cultured in Dulbecco's modified Eagle's medium supplemented with 1% glutamine, 1% antibiotic mix (penicillin–streptomycin) and 10% FBS (Fisher Scientifics, GIBCO). Human normal keratinocytes immortalized by permanent TERT expression (N/TERT-1 cells) were obtained from Dr. James Rheinwald (Harvard Skin Disease Research Center) and cultured according to their protocol (available upon request at their cell culture facility).

Recombinant virus culture

To reconstitute recombinant viruses, 3 μg of the modified BACs per well of 6-well plates were transfected into MeWo cells using 6 μl of JetPEI (PolyPlus transfection), according to the manufacturer's protocol. Three days later, the cells were transferred into a 25 cm^2 flask and passaged near confluence every 2–3 days until typical infection foci appeared.

To infect HFF/MRC5/N/TERT-1 cells, strongly infected MeWo cells were trypsinized and placed in contact with the cells for 20 min. The cells were then washed 3 times with PBS and placed back in the incubator with complete culture medium.

Determination of viral growth

In order to determine the growth kinetics of the different viral recombinant strains, infected MeWo cells were trypsinized on day 0 and the proportion of GFP positive cells, corresponding to infected cells, was determined by FACS (BD CantoII). Four 25 cm^2 flasks of MeWo cells for each viral strain were then infected via co-culture with 200 or 500 infected cells (see figure legend). On day 1–4, one 25 cm^2 flask for each virus was trypsinized and serially diluted (dilution range from 1/36 to 1/1024, performed in triplicates) on 24-well plates containing uninfected MeWo cells. Three days post-seeding, the number of infection foci was recorded in every countable well with an inverted fluorescence microscope. A second measure was carried out on the following day in order to increase accuracy.

Western blotting

Protein samples were incubated with sodium dodecyl sulfate (SDS)-loading buffer (125 mM Tris–HCl [pH 6.8], 4% SDS, 20% glycerol, 6% β-mercaptoethanol, 0.03% bromophenol blue) and boiled for 3 min. Proteins were then separated by SDS-PAGE and transferred onto a polyvinylidene difluoride membrane. Membranes were blocked with 5% nonfat dry milk PBS-Tween and then incubated with anti-GFP antibody (Roche, 1/500). After 3 washes, the membrane was incubated with the appropriate secondary antibody and the proteins of interest were detected using the Amersham ECL western blotting detection reagents kit (GE Healthcare) and the ImageQuant LAS4000 (GE Healthcare).

Immunofluorescence

Coverslips were washed with PBS, fixed for 30 min in 4% paraformaldehyde-PBS, permeabilized in 0.1% Triton X100-PBS and blocked with 10% FBS-PBS. Coverslips were then incubated for 1–2 h with the primary antibody diluted in 10% FBS-PBS as follows: mouse anti-beta-tubulin (1/500, Sigma), rabbit anti-PML (1/50, Santa Cruz), mouse anti-ORF40 (1/50, Santa Cruz), rabbit anti-ORF29 (1/200, kind gift from Dr. R. Cohrs), rabbit anti-ORF45/42 (1/200, kind gift from Dr. R. Visalli) or rabbit anti-ORF33/33.5 (1/50, kind gift from Dr. F. Rixon), rabbit anti-ORF23 (1/200, kind gift from Dr. M. Sommer). After 3 washes in 5% FBS-PBS, coverslips were incubated for 1 h with the appropriate secondary antibody (coupled to Alexa568 or Alexa633, as described in the figure legend) (Invitrogen) diluted 1/400 in 10% FBS-PBS. After washing and nuclei staining with Hoechst33342 (Acros Organics) diluted 1/100,000, coverslips were mounted on glass slides with mowiol. Images were recorded with an Olympus FV1000 confocal inverted microscope using a 63 × oil objective.

Live imaging

A Nikon A1R confocal microscope equipped with a motorized platform and a chamber controlling the temperature, the humidity and the CO_2 level was used for all live imaging experiments. For Fluorescence Recovery After Photobleaching (FRAP) experiments, a region of interest (ROI) was bleached via 488-laser illumination for 45 s at the laser maximum intensity before recording images every 15 s. For Fluorescence Loss in Photobleaching (FLIP), the ROI was first bleached for 1 min before successive pictures acquisition (2 frames each time) followed by 5-seconds photobleaching.

Generation of shPML-MeWo cell line

Retrovirus vectors allowing shPML expression were generated after the transfection of phoenix-Ampho cells (ATCC #SD3443) with the pCKsuper-shPML (kind gift from Dr. C. Kyratsous). The retrovirus vectors were used to transduce MeWo cells that were selected with first 200 and then 500 μg/ml of hygromycin.

Electron microscopy

VZV eGFP-23p-infected wild-type MeWo cells and shPML-MeWo cells were washed in Sörensen's buffer and fixed for 1.5 h at 4 °C with 2.5% glutaraldehyde in a Sörensen 0.1 M phosphate buffer (pH 7.4) and post-fixed for 30 min with 2% osmium tetroxide. After dehydration in graded ethanol, samples were embedded in Epon. Ultrathin sections obtained with a Reichert Ultracut S ultramicrotome were contrasted with uranyl acetate and lead citrate. Observations were made with a Jeol JEM-1400 transmission electron microscope at 80 kV.

Correlative microscopy

MeWo cells grown in a 35 mm glass-bottom dish were infected via cell contact for 48 h with eGFP-ORF23 VZV, washed with PBS and fixed with 4% paraformaldehyde-PBS. In order to reduce the surface of cells to be analyzed, most of the monolayer was scraped off the dish to leave a central small area which was stained with Hoechst (1/100 000 for 5 min), washed 3 times with PBS and visualized by confocal microscopy. An image Z-stack was recorded for each infection focus present on the glass coverslip that was then unglued from the plastic dish via a 10 s contact with methanol. The cells on the coverslip were fixed again for 1 h at room temperature with 2.5% glutaraldehyde in a Sörensen 0.1 M phosphate buffer (pH 7.4) and post-fixed for 30 min with 2%

osmium tetroxide. After dehydration in graded ethanol, samples were embedded in Epon. Serial ultrathin sections obtained with a Reichert Ultracut S ultramicrotome were contrasted and observed as described above. Ultrathin sections were carefully scrutinized and compared with confocal images until a concordance was clearly assessed. Pictures of the chosen area were then systematically recorded on all available sections.

Acknowledgments

This work was supported by the “Fonds pour la Recherche dans l'Industrie et l'Agriculture” (FRIA, Brussels, Belgium), by the University of Liege (Patrimoine ULg) and by the “Fonds National pour la Recherche Scientifique” (FNRS, Brussels, Belgium).

We are very grateful to Dr. Zhu for the BAC-VZV pOka WT and the Biology Research Branch (BRB) at the NCI, Bethesda, Maryland for the pGalK plasmid and for the SW102 bacterial strain. We thank Dr. R. Cohrs for the anti-ORF29 antibody, Dr. F. Rixon and Dr. V. Preston for the anti-ORF33/33.5 antibody, Dr. R. Visalli for the ORF45/42 antibody, Dr. M. Sommer for the ORF23 antiserum, Dr. C. Kyratsous for the pCKsuper-shPML plasmid, Dr. Roger Tsien for the generous gift of the pTag-RFP-T vector, and Dr. F. Patrascu for the HFF cells.

We thank Dr. Y. Habraken, Dr. S. Legrand, Dr. N. Jacobs, Dr. L. Gillet, Dr. J.C. Twizere and Dr. F. Dequiedt for fruitfull interactions and help in the interpretation of the results. We also thank P. Piscicelli for the TEM preparation of samples and C. Lassence and N. Renotte for technical assistance.

Finally, we would like to give our thanks to S. Ormenese, G. Moraes and R. Stephan for FACS analysis and confocal microscopy (Imaging technological platform, GIGA-R), the GIGA-Viral vectors platform for helping with retroviral productions and to C. Lam for DNA sequencing (Genotranscriptomics Platform, GIGA-R).

Appendix A. Supporting information

Supplementary data associated with this article can be found in the online version at http://dx.doi.org/10.1016/j.virol.2014.02.023.

References

Abaitua, F., O'Hare, P., 2008. Identification of a highly conserved, functional nuclear localization signal within the N-terminal region of herpes simplex virus type 1 VP1-2 tegument protein. J. Virol. 82, 5234–5244.
Arvin, A.M., 1996. Varicella-zoster virus. Clin. Microbiol. Rev. 9, 361–381.
Bucks, M.A., O'Regan, K.J., Murphy, M.A., Wills, J.W., Courtney, R.J., 2007. Herpes simplex virus type 1 tegument proteins VP1/2 and UL37 are associated with intranuclear capsids. Virology 361, 316–324.
de Bruyn Kops, A., Knipe, D.M., 1994. Preexisting nuclear architecture defines the intranuclear location of herpesvirus DNA replication structures. J. Virol. 68, 3512–3526.
de Bruyn Kops, A., Uprichard, S.L., Chen, M., Knipe, D.M., 1998. Comparison of the intranuclear distributions of herpes simplex virus proteins involved in various viral functions. Virology 252, 162–178.
Cardone, G., Heymann, J.B., Cheng, N., Trus, B.L., Steven, A.C., 2012. Procapsid assembly, maturation, nuclear exit: dynamic steps in the production of infectious herpesvirions. Adv. Exp. Med. Biol. 726, 423–439.
Chaudhuri, V., Sommer, M., Rajamani, J., Zerboni, L., Arvin, A.M., 2008. Functions of Varicella-zoster virus ORF23 capsid protein in viral replication and the pathogenesis of skin infection. J. Virol. 82, 10231–10246.
Cohrs, R.J., Wischer, J., Essman, C., Gilden, D.H., 2002. Characterization of varicella-zoster virus gene 21 and 29 proteins in infected cells. J. Virol. 76, 7228–7238.
Coller, K.E., Lee, J.I., Ueda, A., Smith, G.A., 2007. The capsid and tegument of the alphaherpesviruses are linked by an interaction between the UL25 and VP1/2 proteins. J. Virol. 81, 11790–11797.
Desai, P., Akpa, J.C., Person, S., 2003. Residues of VP26 of herpes simplex virus type 1 that are required for its interaction with capsids. J. Virol. 77, 391–404.
Desai, P., Person, S., 1998. Incorporation of the green fluorescent protein into the herpes simplex virus type 1 capsid. J. Virol. 72, 7563–7568.
Desai, P., Sexton, G.L., Huang, E., Person, S., 2008. Localization of herpes simplex virus type 1 UL37 in the Golgi complex requires UL36 but not capsid structures. J. Virol. 82, 11354–11361.
Desai, P., Sexton, G.L., McCaffery, J.M., Person, S., 2001. A null mutation in the gene encoding the herpes simplex virus type 1 UL37 polypeptide abrogates virus maturation. J. Virol. 75, 10259–10271.
Desai, P.J., 2000. A null mutation in the UL36 gene of herpes simplex virus type 1 results in accumulation of unenveloped DNA-filled capsids in the cytoplasm of infected cells. J. Virol. 74, 11608–11618.
Feierbach, B., Piccinotti, S., Bisher, M., Denk, W., Enquist, L.W., 2006. Alpha-herpesvirus infection induces the formation of nuclear actin filaments. PLoS Pathog. 2, e85.
Henaff, D., Remillard-Labrosse, G., Loret, S., Lippe, R., 2013. Analysis of the early steps of herpes simplex virus 1 capsid tegumentation. J. Virol. 87, 4895–4906.
Henson, B.W., Perkins, E.M., Cothran, J.E., Desai, P., 2009. Self-assembly of Epstein-Barr virus capsids. J. Virol. 83, 3877–3890.
Homa, F.L., Brown, J.C., 1997. Capsid assembly and DNA packaging in herpes simplex virus. Rev. Med. Virol. 7, 107–122.
Hutchinson, I., Whiteley, A., Browne, H., Elliott, G., 2002. Sequential localization of two herpes simplex virus tegument proteins to punctate nuclear dots adjacent to ICP0 domains. J. Virol. 76, 10365–10373.
Kelly, B.J., Mijatov, B., Fraefel, C., Cunningham, A.L., Diefenbach, R.J., 2012. Identification of a single amino acid residue which is critical for the interaction between HSV-1 inner tegument proteins pUL36 and pUL37. Virology 422, 308–316.
Kinchington, P.R., Bookey, D., Turse, S.E., 1995. The transcriptional regulatory proteins encoded by varicella-zoster virus open reading frames (ORFs) 4 and 63, but not ORF 61, are associated with purified virus particles. J. Virol. 69, 4274–4282.
Klupp, B.G., Fuchs, W., Granzow, H., Nixdorf, R., Mettenleiter, T.C., 2002. Pseudorabies virus UL36 tegument protein physically interacts with the UL37 protein. J. Virol. 76, 3065–3071.
Klupp, B.G., Granzow, H., Mundt, E., Mettenleiter, T.C., 2001. Pseudorabies virus UL37 gene product is involved in secondary envelopment. J. Virol. 75, 8927–8936.
Kobiler, O., Brodersen, P., Taylor, M.P., Ludmir, E.B., Enquist, L.W., 2011. Herpesvirus replication compartments originate with single incoming viral genomes. mBio 2, e00278–11.
Kyratsous, C.A., Walters, M.S., Panagiotidis, C.A., Silverstein, S.J., 2009. Complementation of a herpes simplex virus ICP0 null mutant by varicella-zoster virus ORF61p. J. Virol. 83, 10637–10643.
Lee, J.H., Vittone, V., Diefenbach, E., Cunningham, A.L., Diefenbach, R.J., 2008. Identification of structural protein-protein interactions of herpes simplex virus type 1. Virology 378, 347–354.
Lee, J.I., Luxton, G.W., Smith, G.A., 2006. Identification of an essential domain in the herpesvirus VP1/2 tegument protein: the carboxy terminus directs incorporation into capsid assemblons. J. Virol. 80, 12086–12094.
Lenac Rovis, T., Bailer, S.M., Pothineni, V.R., Ouwendijk, W.J., Simic, H., Babic, M., Miklic, K., Malic, S., Verweij, M.C., Baiker, A., Gonzalez, O., von Brunn, A., Zimmer, R., Fruh, K., Verjans, G.M., Jonjic, S., Haas, J., 2013. Comprehensive analysis of varicella-zoster virus proteins using a new monoclonal antibody collection. J. Virol. 87, 6943–6954.
Luxton, G.W., Haverlock, S., Coller, K.E., Antinone, S.E., Pincetic, A., Smith, G.A., 2005. Targeting of herpesvirus capsid transport in axons is coupled to association with specific sets of tegument proteins. Proc. Natl. Acad. Sci. U.S.A. 102, 5832–5837.
Luxton, G.W., Lee, J.I., Haverlock-Moyns, S., Schober, J.M., Smith, G.A., 2006. The pseudorabies virus VP1/2 tegument protein is required for intracellular capsid transport. J. Virol. 80, 201–209.
Markovitz, N.S., Roizman, B., 2000. Small dense nuclear bodies are the site of localization of herpes simplex virus 1 U(L)3 and U(L)4 proteins and of ICP22 only when the latter protein is present. J. Virol. 74, 523–528.
McNabb, D.S., Courtney, R.J., 1992. Characterization of the large tegument protein (ICP1/2) of herpes simplex virus type 1. Virology 190, 221–232.
Mohl, B.S., Bottcher, S., Granzow, H., Kuhn, J., Klupp, B.G., Mettenleiter, T.C., 2009. Intracellular localization of the pseudorabies virus large tegument protein pUL36. J. Virol. 83, 9641–9651.
Morrison, E.E., Stevenson, A.J., Wang, Y.F., Meredith, D.M., 1998. Differences in the intracellular localization and fate of herpes simplex virus tegument proteins early in the infection of Vero cells. J. Gen. Virol. 79 (Pt 10), 2517–2528.
Nagel, C.H., Dohner, K., Binz, A., Bauerfeind, R., Sodeik, B., 2012. Improper tagging of the non-essential small capsid protein VP26 impairs nuclear capsid egress of herpes simplex virus. PloS One 7, e44177.
Newcomb, W.W., Homa, F.L., Thomsen, D.R., Booy, F.P., Trus, B.L., Steven, A.C., Spencer, J.V., Brown, J.C., 1996. Assembly of the herpes simplex virus capsid: characterization of intermediates observed during cell-free capsid formation. J. Mol. Biol. 263, 432–446.
Newcomb, W.W., Homa, F.L., Thomsen, D.R., Trus, B.L., Cheng, N., Steven, A., Booy, F., Brown, J.C., 1999. Assembly of the herpes simplex virus procapsid from purified components and identification of small complexes containing the major capsid and scaffolding proteins. J. Virol. 73, 4239–4250.
Newcomb, W.W., Trus, B.L., Cheng, N., Steven, A.C., Sheaffer, A.K., Tenney, D.J., Weller, S.K., Brown, J.C., 2000. Isolation of herpes simplex virus procapsids from cells infected with a protease-deficient mutant virus. J. Virol. 74, 1663–1673.
de Oliveira, A.P., Glauser, D.L., Laimbacher, A.S., Strasser, R., Schraner, E.M., Wild, P., Ziegler, U., Breakefield, X.O., Ackermann, M., Fraefel, C., 2008. Live visualization of herpes simplex virus type 1 compartment dynamics. J. Virol. 82, 4974–4990.

Perkins, E.M., Anacker, D., Davis, A., Sankar, V., Ambinder, R.F., Desai, P., 2008. Small capsid protein pORF65 is essential for assembly of Kaposi's sarcoma-associated herpesvirus capsids. J. Virol. 82, 7201–7211.
Quinlan, M.P., Chen, L.B., Knipe, D.M., 1984. The intranuclear location of a herpes simplex virus DNA-binding protein is determined by the status of viral DNA replication. Cell 36, 857–868.
Reichelt, M., Joubert, L., Perrino, J., Koh, A.L., Phanwar, I., Arvin, A.M., 2012. 3D reconstruction of VZV infected cell nuclei and PML nuclear cages by serial section array scanning electron microscopy and electron tomography. PLoS Pathog. 8, e1002740.
Reichelt, M., Wang, L., Sommer, M., Perrino, J., Nour, A.M., Sen, N., Baiker, A., Zerboni, L., Arvin, A.M., 2011. Entrapment of viral capsids in nuclear PML cages is an intrinsic antiviral host defense against varicella-zoster virus. PLoS Pathog. 7, e1001266.
Riva, L., Thiry, M., Bontems, S., Joris, A., Piette, J., Lebrun, M., Sadzot-Delvaux, C., 2013. ORF9p phosphorylation by ORF47p is crucial for the formation and egress of varicella-zoster virus viral particles. J. Virol. 87, 2868–2881.
Salmon, B., Cunningham, C., Davison, A.J., Harris, W.J., Baines, J.D., 1998. The herpes simplex virus type 1 U(L)17 gene encodes virion tegument proteins that are required for cleavage and packaging of viral DNA. J. Virol. 72, 3779–3788.
Smith, G.A., Pomeranz, L., Gross, S.P., Enquist, L.W., 2004. Local modulation of plus-end transport targets herpesvirus entry and egress in sensory axons. Proc. Natl. Acad. Sci. U.S.A. 101, 16034–16039.
Spencer, J.V., Newcomb, W.W., Thomsen, D.R., Homa, F.L., Brown, J.C., 1998. Assembly of the herpes simplex virus capsid: preformed triplexes bind to the nascent capsid. J. Virol. 72, 3944–3951.
Stellberger, T., Hauser, R., Baiker, A., Pothineni, V.R., Haas, J., Uetz, P., 2010. Improving the yeast two-hybrid system with permutated fusions proteins: the Varicella Zoster Virus interactome. Prot. Sci. 8, 8.
Sugimoto, K., Uema, M., Sagara, H., Tanaka, M., Sata, T., Hashimoto, Y., Kawaguchi, Y., 2008. Simultaneous tracking of capsid, tegument, and envelope protein localization in living cells infected with triply fluorescent herpes simplex virus 1. J. Virol. 82, 5198–5211.
Taus, N.S., Salmon, B., Baines, J.D., 1998. The herpes simplex virus 1 UL 17 gene is required for localization of capsids and major and minor capsid proteins to intranuclear sites where viral DNA is cleaved and packaged. Virology 252, 115–125.
Thomsen, D.R., Newcomb, W.W., Brown, J.C., Homa, F.L., 1995. Assembly of the herpes simplex virus capsid: requirement for the carboxyl-terminal twenty-five amino acids of the proteins encoded by the UL26 and UL26.5 genes. J. Virol. 69, 3690–3703.
Trus, B.L., Booy, F.P., Newcomb, W.W., Brown, J.C., Homa, F.L., Thomsen, D.R., Steven, A.C., 1996. The herpes simplex virus procapsid: structure, conformational changes upon maturation, and roles of the triplex proteins VP19c and VP23 in assembly. J. Mol. Biol. 263, 447–462.
Trus, B.L., Newcomb, W.W., Cheng, N., Cardone, G., Marekov, L., Homa, F.L., Brown, J. C., Steven, A.C., 2007. Allosteric signaling and a nuclear exit strategy: binding of UL25/UL17 heterodimers to DNA-Filled HSV-1 capsids. Mol. Cell 26, 479–489.
Ward, P.L., Ogle, W.O., Roizman, B., 1996. Assemblons: nuclear structures defined by aggregation of immature capsids and some tegument proteins of herpes simplex virus 1. J. Virol. 70, 4623–4631.
Warming, S., Costantino, N., Court, D.L., Jenkins, N.A., Copeland, N.G., 2005. Simple and highly efficient BAC recombineering using galK selection. Nucl. Acids Res. 33, e36.